Room Temperature and Shock Tube Study of the Reaction HCO + O_2 Using the Photolysis of Glyoxal as an Efficient HCO Source

M. Colberg and G. Friedrichs*

Institut für Physikalische Chemie, Olshausenstr. 40, Christian-Albrechts-Universität zu Kiel, D-24098 Kiel, Germany

Received: September 13, 2005; In Final Form: October 17, 2005

The rate of the reaction 1, HCO + O_2 → HO_2 + CO, has been determined (*i*) at room temperature using a slow flow reactor setup (20 mbar < p < 500 mbar) and (*ii*) in the temperature range 739 K < T < 1108 K behind reflected shock waves (0.82 bar < p < 1.84 bar) employing a perturbation approach. Following the 193 nm excimer laser photolysis of mixtures of glyoxal in Ar, concentration−time profiles were measured using frequency modulation (FM) detection of HCO at a wavelength of $\lambda = 614.752$ nm. Observed differences between HCO concentration−time profiles measured with and without O_2 added to the reaction mixtures could be almost exclusively attributed to reaction 1. The determined rate constants, $k_1(295\ \text{K}) = (3.55 \pm 0.05) \times 10^{12}$ cm^3 mol^{-1} s^{-1}, $k_1(739-1108\ \text{K}) = 3.7 \times 10^{13} \exp(-13\ \text{kJ mol}^{-1}/RT)$ cm^3 mol^{-1} s^{-1} ($\Delta \log k_1 = \pm 0.16$), reveal a slightly positive temperature dependence of reaction 1 at high temperatures. Furthermore, the 193 nm photolysis of glyoxal, $(CHO)_2$, has been proven to be an efficient HCO source. Besides HCO, photolysis of the precursor also produces H atoms. The ratio of initially generated H atoms and HCO radicals, $f = [H]_0/[HCO]_0^{\text{total}}$, was found to depend on the total density ρ. At room temperature, it varies from $f = 1.6$ at $\rho = 8 \times 10^{-7}$ mol cm^{-3} to $f = 3.0$ at $\rho = 2 \times 10^{-5}$ mol cm^{-3}. H atoms are transformed via reaction 4, H + $(CHO)_2$ → H_2 + HCO + CO, into additional HCO radicals. The rate constants of reaction 4 were determined from unperturbed photolysis experiments to be $k_4(295\ \text{K}) = (3.6 \pm 0.3) \times 10^{10}$ cm^3 mol^{-1} s^{-1} and $k_4(769-1107\ \text{K}) = 5.4 \times 10^{13} \exp(-18\ \text{kJ mol}^{-1}/RT)$ cm^3 mol^{-1} s^{-1}($\Delta \log k_4 = \pm 0.12$).

1. Introduction

The formyl radical, HCO, plays an important role in combustion chemistry. In hydrocarbon oxidation, it is mainly formed by the attack of formaldehyde by free atoms or radicals, e.g. (H, OH) + CH_2O → (H_2, H_2O) + HCO, and the reaction of O atoms with ethylene, O + C_2H_4 → CH_3 + HCO. The fate of the formyl radicals, which largely determines the overall oxidation rate of CH_2O,[1] is dominated by the two major removal channels

$$\text{HCO} + \text{O}_2 \rightarrow \text{HO}_2 + \text{CO} \quad (1)$$

$$\text{HCO} + \text{M} \rightarrow \text{H} + \text{CO} + \text{M} \quad (2)$$

Whereas the high-temperature rate and the pressure dependence of the unimolecular decomposition reaction 2 have been subject of several recent studies,[2−5] direct measurements of the rate constant of reaction 1 are still limited to temperatures lower than 713 K. Preceding experimental studies revealed a slightly negative,[6,7] positive,[8] or negligible[9] temperature dependence of the rate constant k_1, thus resulting in considerable uncertainty of the extrapolated high temperature rate constant. An overall small temperature dependence, however, is consistent with an association−elimination mechanism. The initially formed activated association complex $HC(O)O_2$* can rapidly dissociate into HO_2 and CO in a concerted manner.[10] The alternative direct abstraction reaction, which also yields HO_2 and CO, would result in a positive temperature dependence. According to variational transition state calculations of Hsu et al.,[10] the direct abstraction process cannot compete with the association−elimination mechanism at temperatures below 1000 K. In contrast to the HO_2 and CO forming channel, the more exothermic decomposition channel with CO_2 + OH as products requires a preceding H migration step of the $HC(O)O_2$* intermediate over a significant energy barrier. Experimentally, Temps and Wagner[11] and Yamasaki et al.[12] set the upper limit of this OH forming channel to <0.4% and <0.3%, respectively. Also the formation of collisional stabilized adduct is unlikely except at extremely high pressures. Both experimental[6,13,14] and theoretical[10,15] work agree that there is no discernible pressure dependence of the reaction up to pressures of several bar. Thus, for most practical high-temperature applications, reaction 1 can be treated as a simple second-order reaction with HO_2 + CO as the exclusive products.

In contrast to the assumed products, the high-temperature rate constants used in modeling studies are less consistent. For example, at $T = 2000$ K the rate expression accepted for the detailed GRI Mech 3.0 natural gas combustion mechanism,[16] which is known to be capable of a reliable representation of natural gas flames and ignition over a wide range of temperatures and pressures, places the rate of reaction 1 a factor of 1.8 higher than the extrapolated upper limit of existing direct measurements. Recently, Glarborg et al.[1] proposed a detailed reaction mechanism for the oxidation of formaldehyde under postflame conditions, which was tested against flow reactor studies performed at temperatures between 800 and 1400 K under fuel-rich and very lean conditions. Compared to the GRI Mech 3.0 recommendation, their data could be well represented by adopting a roughly two times lower rate constant for the

* To whom correspondence should be addressed. E-mail: gfriedr@phc.uni-kiel.de.

10.1021/jp055168r CCC: $33.50
Published on Web 12/09/2005

unimolecular decomposition of HCO from Friedrichs et al.[2] and a factor of 3.3 lower rate constant for reaction 1 from DeSain et al.[9] High temperature experimental data for the title reaction are clearly needed to resolve remaining discrepancies.

The investigation of HCO reactions at high temperatures is difficult due to the high reactivity and thermal instability of HCO, which causes its lifetime to be short and the observable concentration levels to be low. Whereas the problem of low intermediate concentrations can be overcome by a sensitive detection method, frequency modulation (FM) spectroscopy in our case, suitable HCO sources for high temperature kinetic measurements are not readily available. So far, the detection of HCO behind shock waves was limited to studies of the formaldehyde reaction system. In that work, HCO was generated either by photolysis or direct pyrolysis of formaldehyde.[2,3] At $p = 1$ bar and $T = 1000$ K, the lifetime of HCO of $\tau \approx 4$ μs due to its fast thermal decomposition is already close to the time resolution attainable in practical shock tube experiments. Due to the rovibrational relaxation of initially formed excited HCO (in case of photolysis experiments), or due to the passage time of the shock wave through the line-of-sight of the detection laser (in case of pyrolysis experiments), a reasonable minimum time resolution is in the order of 0.5−2 μs. Therefore, the detection of HCO behind shock waves strongly relies on a regeneration mechanism for HCO radicals. In the case of formaldehyde, the chain reaction

$$HCO + M \rightarrow H + CO + M \quad (2)$$

$$H + CH_2O \rightarrow H_2 + HCO \quad (3)$$

steadily converts formaldehyde into HCO radicals. In the present work, we now employed the photolysis of glyoxal, $(CHO)_2$, as a new HCO high-temperature source for shock tube measurements. Besides HCO, photolysis of the precursor at a wavelength of $\lambda = 193$ nm also produces hydrogen atoms. The subsequent abstraction reaction of the H atoms with glyoxal initially yields the unstable (CHO)CO radical.

$$H + (CHO)_2 \rightarrow H_2 + (CHO)CO \rightarrow H_2 + HCO + CO \quad (4')$$

Since (CHO)CO rapidly decomposes within the time resolution of the experiments,[17] similar to reaction 3 in the formaldehyde case, reaction 4′ acts as a permanent HCO source in the glyoxal system.

In this work, the 193 nm photolysis of glyoxal was investigated at room temperature and at temperatures 769 K < T < 1107 K behind shock waves. From experiments with mixtures of glyoxal in argon, the rate constant of reaction 4′ and the H atom photolysis yield were determined. The observed HCO profiles can be described by a consistent mechanism. Subsequently, the room temperature and high temperature (739 K < T < 1108 K) rate constants of the title reaction 1 were measured by a perturbation approach. Observed differences between HCO profiles measured with and without O_2 added to the reaction mixtures could be attributed almost exclusively to reaction 1.

2. Experimental Section

2.1. Shock Tube and Slow Flow Reactor. The high temperature experiments were performed behind reflected shock waves using a recently remodeled high purity shock tube originally designed for atom-resonance-absorption-spectroscopy.[18] The mostly metal-sealed stainless steel shock tube with an inner diameter of 81 mm (10 mm wall thickness) was driven with hydrogen or hydrogen/nitrogen mixtures as the driver gas and had a driver length of 3.7 m. Typical operating conditions using 50−100 μm thick aluminum diaphragms were 700 K < T < 3500 K and 0.75 bar < p < 3.5 bar. The electropolished test section with a total length of 4.4 m could be evacuated down to pressures of $p \approx 10^{-7}$ mbar with a turbomolecular drag/diaphragm backing pump combination (oil free vacuum, Pfeiffer TMU261/MVP055-3) at a combined leak and outgassing rate of 3×10^{-6} mbar/min. The incident shock velocity was measured with four fast piezoelectric pressure transducers. The last transducer was installed together with two optical ports at a distance of 19 mm from the end wall. The average attenuation of the incident shock velocity was found to be 1.5% per meter. Reflected shock pressures and temperatures were calculated from the shock velocity extrapolated to the endwall using a frozen chemistry, one-dimensional shock tube code in conjunction with thermodynamic data taken from the Konnov and TRC databases.[19,20] A small, independent correction in order to account for boundary layer perturbations has been applied. Detailed test measurements using the thermal decomposition of methylamine and ammonia as benchmark systems showed that the calculated ideal temperature was too low by 1−1.5%. Furthermore, the experimental pressure, which was deduced from the ratio of the pressures measured behind the reflected and incident shock wave, was always slightly higher (≈3%) than predicted by ideal theory. The results of these test measurements, which will be published elsewhere,[21] could be nicely reproduced by a correction procedure based on Mirels's boundary layer theory as given by Michael and Sutherland.[22,23] Consequently, we applied the corrections for nonideality both to pressure and temperature behind the reflected shock wave. The introduced corrections, however, are close to the accuracies of the one-dimensional shock wave calculations.

Room-temperature measurements have been performed by using the shock tube itself as a quasi-static cell or, alternatively, by using a 45 cm long slow flow reactor made out of glass equipped with quartz windows.

2.2 Photolysis. The photolysis of the reaction mixtures was performed collinearly with the detection laser beam using an optical setup with two dichroic mirrors. An ArF excimer laser (Lambda Physik EMG100) was used to generate HCO radicals and H atoms by photolysis of glyoxal at $\lambda = 193$ nm. Average energy fluences of 10 and 60 mJ $cm^{-2}pulse^{-1}$ were maintained in the slow flow cell and shock tube, respectively, as could be estimated from the photolysis area, the transmission of the windows and the total pulse energy measured using a pyroelectric energy meter (Coherent LM-P10). For the shock tube experiments, the output of the excimer laser was slightly focused through the shock tube windows using a 1 m focusing lens placed 55 cm in front of the entrance window (*side-on* photolysis). Due to the focusing of the photolyis beam, the energy fluence linearly increased over the width of the shock tube by approximately 30% resulting in a nonuniform absolute yield of photolysis products. Such nonuniform concentration profiles could eventually spoil a simple data analysis. However, the increase of energy flux was effectively compensated by a rather strong attenuation of the photolysis laser intensity due to glyoxal absorption. An estimation based on the photolysis model described by Davidson et al.[24] showed that under typical experimental conditions with 1% glyoxal ($\sigma_{193\ nm} \approx 4.8 \times 10^{-19}$ cm^2/molecule) at $T = 1000$ K and $p = 1$ bar the photolysis beam was attenuated by 25% across the shock tube such that the observed line-of-sight absorption signals could be analyzed by simply assuming an average initial H and HCO concentration. Care was also taken to keep the photolysis volume large and

the detection volume small enough in order to ensure a negligible concentration change due to radial diffusion.

2.3. Gas Mixtures. Glyoxal samples were prepared by heating glyoxal trimeric dihydrate in the presence of P_2O_5 and were stored in liquid nitrogen. No impurities could be detected using FTIR. Gas mixtures of typically 0.5−2% glyoxal in Ar were prepared manometrically in a 18 L stainless steel mixing vessel. The mixing vessel and the gas handling manifold were routinely evacuated to pressures of $p < 10^{-5}$ mbar with a turbomolecular drag/diaphragm backing pump combination (oil free vacuum, Pfeiffer TMU71/MVP015-2) prior to mixture preparation. 5% of He was added to the mixtures in order to shorten the vibrational relaxation time of O_2 if necessary. The mixtures were used within a few days after preparation; no noticeable change in the experimental HCO signals was discernible with increasing reaction mixture age. Where required, controlled levels of oxygen were added to the mixtures or the mixtures were further diluted with Ar by using a flow system with calibrated mass flow controllers (Aera, FC series). The mixtures were let into the shock tube through a small valve which was mounted flush to the end wall of the test section of the shock tube. Typically, the reaction mixture was slowly pumped through the shock tube at the particular test pressure for 3 min in order to eliminate any wall adsorption effects. The gases and chemicals used were Ar (99.999%), He (99.996%), H_2 (99.993%, as driver gas), O_2 (99.995%), and glyoxal trimeric dihydrate (>97%).

2.4. Frequency Modulation Detection of HCO. HCO was detected by means of frequency modulation (FM) spectroscopy, the state-of-the-art sensitive laser absorption method for small radicals behind shock waves.[2,25,26] Quantitative detection of HCO was performed on the blended, with 0.3 cm^{-1} moderately lifetime broadened Q(6)P(1) absorption line of the ($\tilde{A}^2A'' \leftarrow \tilde{X}^2A'$)($09^00 \leftarrow 00^10$) transition at a wavelength of $\lambda = 614.752$ nm. The FM spectrometer used was similar to the setup described in refs 2 and 26. Briefly, the wavelength of a Nd:YVO_4 solid-state laser (Coherent Verdi-V10) pumped *cw* ring-dye laser (Coherent 899−21, line width ≈100 kHz) was measured by a wavemeter (MetroLux WL200) with an absolute accuracy of 200 MHz. The laser light was modulated at a frequency of 1.0 GHz using a resonant electrooptic modulator (New Focus 4421). Modulation indices of $M = 1.2-1.7$ were measured using a scanning etalon (Coherent SM 240-1 B). The laser beam passed through the shock tube and was detected by a fast photodiode (Hamamatsu S5973). About 10−20 mW total optical power was maintained at the detector. A voltage controlled phase-shifter (Lorch) in combination with a two polarizer setup[2] was used to set the phase angle of demodulation to zero, resulting in purely absorption induced FM signals. The demodulated FM signal, I_{FM}, which is proportional to the concentration c of the absorbing species according to[2,26]

$$I_{FM} = \frac{I_0}{2} \times \Delta f \times \sigma\, c\, l \times G \qquad \text{(I)}$$

was stored in a digital oscilloscope (Hameg HM507, 8 bit, typically 10MS/s) and was filtered using a Butterworth digital filter set to a time resolution of approximately 0.5−0.7 μs. Here, I_0 is the total light intensity, σ the narrow-bandwidth absorption cross section, l the absorption path length, and G the electronic gain of the FM spectrometer. Whereas Δf, the FM factor, can be calculated from line width data, for a quantitative detection of HCO the gain factor has to be determined experimentally.[26] In this work, G has been measured by three different methods, (*i*) by direct calibration of the FM signal detecting a species with known line shape and absorption cross section, (*ii*) simultaneous measurement of the FM signal and a normal absorption signal, and (*iii*) by using the scanning etalon setup. For method (*i*), high-temperature experiments with known NH_2 radical concentrations were performed. Method (*ii*) was employed by a simultaneous measurement of the FM and conventional absorption signal during a high-resolution scan over a well resolved absorption line of iodine. A simple low-pressure iodine cell was used as the absorbing sample. Figure 1 depicts a measured FM line shape of a iodine absorption line, which was used to deduce the FM factor. Knowing the total intensity I_0, the line shape and the peak absorption of the corresponding absorption signal, the gain factor can be directly obtained from eq I. This simple procedure allows an accurate determination of G provided that both the iodine line and the FM electronics are not saturated. Altogether, as a consensus value of all three methods, $G = 240 \pm 10$ was obtained in this work.

Absolute concentrations of HCO were calculated based on the accurate line shape data and absorption cross sections determined previously.[2] Additionally, allowance was made for a small pressure broadening effect according to an assumed pressure broadening coefficient $\Delta\nu_p = 2.0 \times (T/298\ \text{K})^{-0.75}$ GHz/bar. The uncertainty of the calculated HCO concentrations including the errors of the temperature-dependent absorption cross section and the gain factor can be estimated to be ±25%. Typically, with a maximum FM factor of $\Delta f = 0.3$ at 900 K and 1 bar and the time resolution set to 0.7 μs, an HCO detection limit of 5×10^{-11} mol/cm^3 (3.5 ppm) was achieved behind shock waves.

Some care had to be taken when utilizing high intensity pulsed laser radiation in connection with FM detection. In some cases, in particular when using light absorbing optics like a UV filter, a residual baseline shift of the FM signal was observed following the excimer laser pulse. These baseline shifts, which are probably due to an excimer laser induced heating of the optics, finally limit the smallest detectable absorption. The effect can be minimized by tilting the corresponding optical components or even avoided by using reflective optics. Test measurements with pure argon were always performed in order to guarantee an accurate baseline.

2.5. Numerical Simulations. The HCO concentration−time profiles were numerically simulated using our previously validated formaldehyde submechanism.[3] The GRI Mech 3.0 mechanism[16] has been applied as a base mechanism in order to include potential secondary chemistry. The rate constants of the following key reactions,

$$H + HCO \rightarrow H_2 + CO \qquad (5)$$

$$HCO + HCO \rightarrow CH_2O + CO \qquad (6)$$

$$HCO + M \rightarrow H + CO + M \qquad (2)$$

have been adopted from our previous study and are summarized together with other important reactions in Table 1. Whereas the rate constants for reactions 5 and 6 are close to recommended values,[31,32] the used rate constants for the unimolecular decomposition of HCO are roughly a factor of 2 lower than the values derived from the work of Timonen et al.,[33] which are commonly used in reaction mechanisms for hydrocarbon oxidation. Our recommended rate expression for the rate constant of reaction 2 is in excellent agreement with the results of recent direct measurements of Krasnoperov et al.,[5] but also recently Hippler et al. reported high-pressure data on reaction 2 that again support the higher rate constants of Timonen et al. According to an

TABLE 1: Important Reactions for the Evaluation of the Glyoxal Photolysis Experiments[a]

no.	reaction	A	n	E_a	T	
1	HCO + O_2 ⇌ HO_2 + CO	3.55×10^{12}			295	this work
		3.7×10^{13}		13	739−1108	this work
2	HCO + M ⇌ H + CO + M	4.0×10^{13}		65.0	835−1230	ref 2
3	H + CH_2O ⇌ H_2 + HCO	5.74×10^{7}	1.9	11.5	250−5000	refs 27, 28
4	H + $(CHO)_2$ → H_2 + HCO + CO	3.6×10^{10}			295	this work
		5.4×10^{13}		18	295−1107	this work
5	H + HCO ⇌ H_2 + CO	1.1×10^{14}			295−2100	refs 2, 3
6	HCO + HCO ⇌ CH_2O + CO	2.7×10^{13}			295−2100	refs 3, 11
7	HCO* + M → HCO + M	1.6×10^{11}			295	this work
8	HCO + $(CHO)_2$ → products		$k_4/40$		700−1150	estimated
9	H + HO_2 ⇌ OH + OH	4.3×10^{13}			295	ref 29
		8.4×10^{13}		2.7	700−1150	ref 16
10	OH + $(CHO)_2$ → H_2O + HCO + CO	6.4×10^{12}			295	ref 30
		1.3×10^{13}			700−1150	estimated
11	HCO + HO_2 → H + OH + CO_2	3.0×10^{13}			300−2500	ref 31

[a] The GRI Mech 3.0 mechanism[16] has been used as a base mechanism in order to include potential secondary chemistry. At room temperature, supplement reactions of the vibrationally excited HCO* were taken into account by assuming the same rate constants as for the thermally equilibrated HCO (see text). A double arrow indicates that the reverse reaction has been also taken into account. Rate constants are given as $k_i = AT^n \exp(-E_a/RT)$ (units kJ, cm^3, mol, s, and K).

isolated resonance model applied by Hippler et al.,[4,34] the apparant discrepancies can be traced back to a weak falloff effect. They found that the experimental k_2 values roughly scale with $[M]^{0.87}$ such that the reported discrepancies reduce to the uncertainty limits set by the different studies. Since the validated results of our previous study[2,3] have been obtained at a comparable temperature range and with the same bath gas as used in this study, for an accurate representation of the high temperature data we rely on our rate expression as given in Table 1.

For all numerical simulations, the Chemkin-II package[35] was used. Where applicable, rate constants for reverse reactions were calculated automatically on the basis of thermodynamic data taken from Konnov,[19] except for glyoxal.[20] For sensitivity analysis the sensitivity coefficient $\sigma(i, j)$ of the i-th reaction of species j was normalized with respect to the maximum concentration of the species j over the time history.

3. Glyoxal Photolysis

At a photolysis wavelength of $\lambda = 193$ nm ($E_{photolysis} = 620$ kJ/mol) the following photodissociation pathways of glyoxal are thermodynamically accessible:

$$(CHO)_2 + h\nu \rightarrow CH_2O + CO \qquad \Delta_r H^\circ_{298} = -14 \text{ kJ/mol}$$
$$\rightarrow H_2 + 2\,CO \qquad \Delta_r H^\circ_{298} = -9 \text{ kJ/mol}$$
$$\rightarrow 2\,HCO \qquad \Delta_r H^\circ_{298} = 299 \text{ kJ/mol}$$
$$\rightarrow HCO + H + CO \qquad \Delta_r H^\circ_{298} = 363 \text{ kJ/mol}$$
$$\rightarrow 2\,H + 2\,CO \qquad \Delta_r H^\circ_{298} = 427 \text{ kJ/mol}$$

A peak HCO quantum yield of $\phi \approx 2$ is observed at photolysis wavelengths around $\lambda = 390$ nm.[36] With increasing photolysis energies, the HCO quantum yield decreases due to the opening of additional glyoxal photolysis pathways and is $\phi = (0.69 \pm 0.29)$ at $\lambda = 308$ nm and $\phi = (0.42 \pm 0.21)$ at $\lambda = 193$ nm.[37] Although quantitative H atom yields have not been measured yet, it is reasonable to assume that the H atom yield will increase at shorter photolysis wavelengths at the expense of the HCO yield. Since both the absorption cross section, $\sigma((CHO)_2, 193\text{ nm}) = 4.8 \times 10^{-19}$ cm^2/molecule,[37] and the expected H atom yield are high, the 193 nm excimer laser photolysis of glyoxal can be expected to constitute an excellent HCO source for high-temperature measurements. For a comparison, the photolysis of formaldehyde at $\lambda = 308$ nm, which is also known to generate both HCO and H atoms with high quantum yields of $\phi = 0.8$ (ref 38), due to its lower absorption cross section of $\sigma(CH_2O, 308\text{ nm}) = 1.4 \times 10^{-20}$ cm^2/molecule,[39] is a much less favorable HCO source.

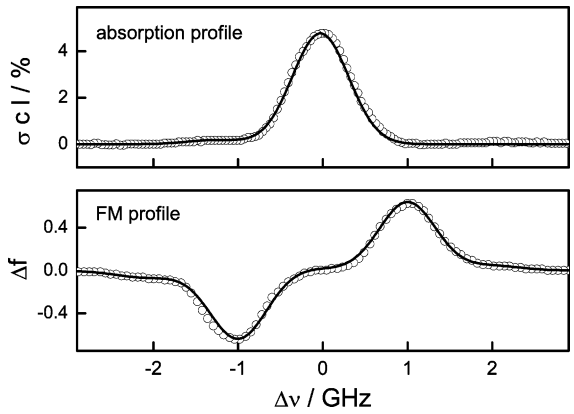

Figure 1. Determination of the gain factor G by direct comparison of absorption and FM data obtained by a high-resolution scan over an iodine absorption line. Modulation frequency $\nu_m = 1.0$ GHz, modulation index $M = 0.72$.

3.1. Room-Temperature Measurements. HCO was detected at room temperature following the photolysis of mixtures of glyoxal in argon at pressures of 20 mbar $< p <$ 525 mbar. The initial glyoxal concentration was varied in the range 8×10^{-9} mol/$cm^3 < [(CHO)_2]_0 < 4 \times 10^{-7}$ mol/cm^3. Figure 2 displays two experimental HCO profiles that have been obtained at the same total pressure of $p = 80$ mbar but with different initial concentrations of glyoxal. For the experiment with 2.8% glyoxal, the excimer laser photolysis energy has been lowered such that the initial HCO concentration was approximately the same as for the 1.6% experiment. The photolysis instantaneously yields HCO followed by an apparent formation of additional HCO during the first few μs. As in the case of formaldehyde photolysis,[2,40] this initial increase of the HCO profiles can be attributed to a relatively slow relaxation of initially formed excited HCO* radicals and can be efficiently modeled by assuming the relaxation reaction

$$HCO^* + M \rightarrow HCO + M \qquad (7)$$

Additional reactions of the excited HCO* radical, H + HCO*, HCO + HCO*, and HCO* + HCO*, were also included in the

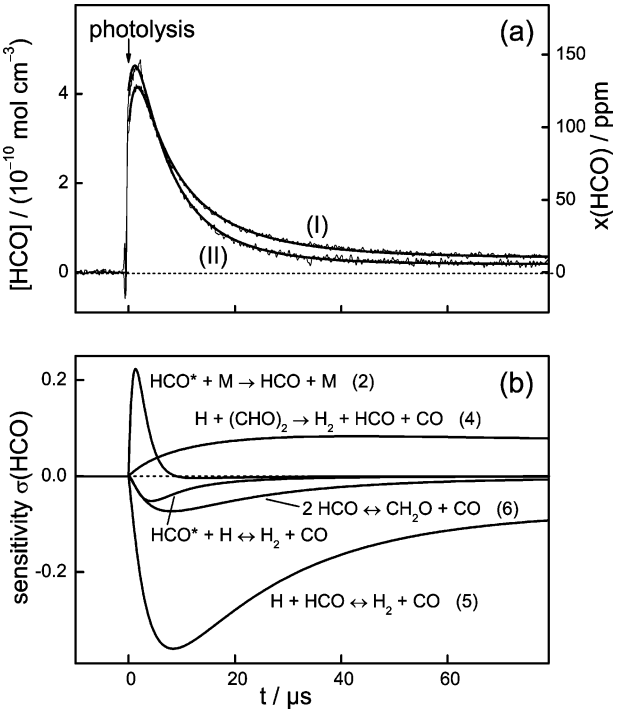

Figure 2. Room temperature determination of the rate constant of reaction 4, H + $(CHO)_2$. (a) Eight times averaged concentration−time profiles for two photolysis experiments at T = 295 K, p = 80 mbar, and initial glyoxal mole fractions of (I) 2.8% and (II) 1.6% in argon. (b) Sensitivity analysis for experiment I.

reaction mechanism by assuming the same rate constants as for the thermally equilibrated HCO. This approximate treatment, which does not take into account possible rate enhancement or attenuation effects of vibrationally excited HCO* radicals, is reasonable due to the overall small influence of these reactions. By fitting the initial increase and the observed HCO maxima, an average relaxation rate constant of $k_7 = 1.6 \times 10^{11}$ cm^3 mol^{-1} s^{-1} and an initial ratio of $[HCO^*]_0/[HCO]_0 \approx 1$ were inferred from the room-temperature experiments, thus similar to the values obtained for formaldehyde photolysis.[2] Moreover, the experimental absolute HCO concentrations, $[HCO]_0^{total} = [HCO]_0 + [HCO^*]_0$, agreed well within ±30% with an estimation of the HCO yield based on the photolysis laser energy fluence and a quantum yield of $\phi(HCO) = 0.42$.

3.1.1. Reaction H + (CHO)$_2$ at Room Temperature. The initial relaxation process is followed by a rapid HCO radical consumption that cannot be explained by the self-reaction 6 of two HCO radicals alone. Instead, as a consequence of a high H atom photolysis yield, the observed fast HCO signal decrease is a direct indication for reaction 5, H + HCO. At high H atom concentrations, however, also the HCO regenerating reaction 4′ becomes feasible:

$$H + (CHO)_2 \rightarrow H_2 + (CHO)CO \rightarrow H_2 + HCO + CO \quad (4')$$

As mentioned above, measurements of Orlando and Tyndall[17] showed that the initially formed (CHO)CO rapidly decomposes. At room temperature and pressures of 175 Torr < p < 700 Torr, the thermal dissociation was found to take place near the low-pressure limit with a pseudo first-order rate constant of $k = 3.5 \times 10^7$ s^{-1} at p = 700 Torr. The reported rate constant corresponds to short lifetimes of 58 ns < τ < 1.4 μs at total pressures of 500 mbar > p > 20 mbar. Hence, for the purpose

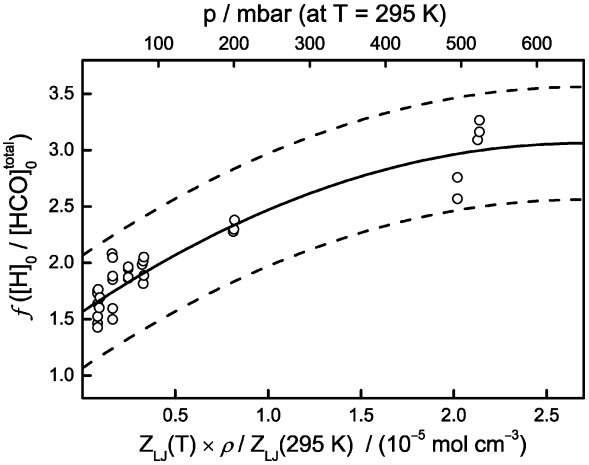

Figure 3. The 193 nm photolysis of glyoxal. H atom yield versus total pressure p (upper axis, at room temperature) and normalized collision frequency (lower axis) in terms of the initial ratio $f = [H]_0/[HCO]_0^{total}$. Z_{LJ} is the Lennard−Jones collision frequency.[44] The dashed curves indicate the estimated error limits of $f \pm 0.5$.

of this study, reaction 4′ could be treated as a direct HCO source according to reaction 4:

$$H + (CHO)_2 \rightarrow H_2 + HCO + CO \quad (4)$$

In Figure 2, the observed deceleration of the HCO consumption at longer reaction times that almost gives rise to HCO "plateaus" is due to the HCO regeneration via reaction 4. The expected increase of the plateau concentration with increasing glyoxal concentration was clearly observed. Knowing the rate constant of reaction 5, it was possible to deduce both the H atom photolysis yield and the rate constant of the reaction 4 from the experimental HCO profiles. The sensitivity analysis shown in the lower part of Figure 2 reveals that the HCO signal decrease at intermediate reaction times is mainly determined by reaction 5 (so the assumed H atom concentration) whereas reaction 4 steadily gains importance and ultimately dominates the HCO plateau concentration at long reaction times. The following room-temperature rate constant was obtained for reaction 4:

$$k_4(295\ K) = (3.6 \pm 0.3) \times 10^{10}\ cm^3\ mol^{-1}\ s^{-1}$$

Here, the error limit corresponds to the error of the mean of 33 measurements based on a 2σ confidence level. Experimental data and conditions are listed in Table 1S in the Supporting Information.

3.1.2. H Atom Photolysis Yield. Based on the determined initial $[HCO]_0$, $[HCO^*]_0$, and $[H]_0$ concentrations, the ratio $f = [H]_0/[HCO]_0^{total}$ could be specified. As outlined in Figure 3, the ratio f was found to depend on the total density ρ. At room temperature, it increases from $f \approx 1.6$ at $\rho = 8 \times 10^{-7}$ mol/cm^3 to $f \approx 3.0$ at $\rho = 2 \times 10^{-5}$ mol/cm^3, respectively.

It is tempting to ascribe this tendency to missing reactions in the reaction mechanism or the approximate treatment of the HCO* chemistry. However, experiments at different inital glyoxal concentrations (varied by a factor of 50) and different inital HCO concentrations (varied by a factor of 85) ensured the consistency of the applied reaction mechanism. As it becomes apparant from the experimental HCO profile shown in Figure 4, the mechanism reproduces the initial signal increase (t < 3 μs), its intermediate decrease (3 μs < t < 15 μs), the

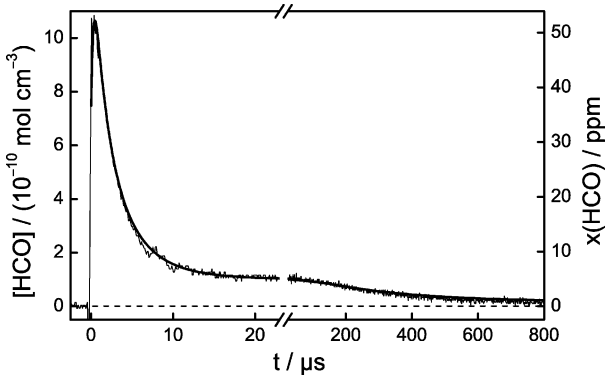

Figure 4. HCO concentration−time profile for an experiment at T = 295 K, p = 500 mbar, and 1.9% glyoxal in argon. The break in the time scale at t = 22 μs was introduced in order to illustrate the long-term behavior of the HCO signal.

apparent plateau at reaction times of 15 μs < t < 80 μs and also the final long-term consumption (t > 80 μs) of the HCO radicals.

Even at the lowest pressures used, the influence of HCO* chemistry is limited to the very early part of the observed HCO profiles. Besides reaction 7, the only other important HCO* reaction which has a slight influence on the modeled HCO concentration is the reaction H + HCO* (see Figure 2b). Simulations with the rate constant of that reaction varied by a factor of 2 revealed that at p = 80 mbar the determined ratio f changed by merely 5%, which is well within the scatter of the data shown in Figure 3.

Possible remaining minor flaws in the mechanism could be induced by the branching fraction of the self-reaction of two HCO radicals, reactions 6 and 6′, and the reaction of HCO radicals with $(CHO)_2$, reaction 8.

$$HCO + HCO \rightarrow CH_2O + CO \quad (6)$$

$$HCO + HCO + M \rightarrow (CHO)_2 + M \quad (6')$$

$$HCO + (CHO)_2 \rightarrow \text{products} \quad (8)$$

However, no pressure dependence of the total rate constant of the association−elimination reaction HCO + HCO with its energetically low-lying exit channel 6 is expected. Also experiments indicate that the deactivation channel 6′ plays a minor role under the experimental conditions used in this work. From a product study of the photolysis of *n*-butanal at p = 100 Torr, Förgeteg et al.[42] concluded a ratio $k_6/k_6' \approx 17$. At room temperature, a significant influence of reaction 8 is very unlikely as well. The simple H-abstraction reaction forming CH_2O + (CHO)CO, which is much less exothermic ($\Delta_r H^\circ_{298} \approx -21$ kJ/mol) than the corresponding H atom reaction 4 ($\Delta_r H^\circ_{298}$ = −79), is expected to exhibit a significant activation barrier.

Next to mechanistic reasons, also a pronounced pressure broadening effect of the HCO absorption feature may have caused the observed pressure dependence of *f*. As noted above, a pressure broadening coefficient of $\Delta\nu_p$ = 2 GHz/bar was used to calculate the absolute HCO concentrations at room temperature. Detailed modeling showed that increasing $\Delta\nu_p$ by an unrealistic factor of 5 could account for most of the observed pressure effect only at the expense of inconsistent rate constants for reaction 4. Moreover, such a high pressure broadening would have significantly influenced the observed absorption line shape, which was confirmed to be consistent with $\Delta\nu_p$ = 2 GHz/bar.

Having excluded mechanistic and concentration issues, the observed pressure dependence of the ratio *f* has to be ascribed to pressure quenching effects. Most probably, the increase of *f* with increasing pressure is due to an increase of the H atom yield at the expense of the HCO radical yield; however, no final conclusion on absolute quantum yields can be drawn from our relative *f* data. The photodissociation of glyoxal, which is known to exhibit a distinct wavelength and pressure dependence, has been subject to several studies. For a short summary, we refer to a recent paper of Chen and Zhu.[36] These authors investigated the photolysis of glyoxal at wavelengths of 290 nm < λ < 420 nm and reported both an efficient quenching of excited glyoxal by ground-state glyoxal in the 320−420 nm region and by nitrogen in the 380−420 nm region. The wavelength and pressure dependence originates from a complex interaction of excited singlet and triplet states, internal conversion, and (collision-induced) intersystem crossing. In our case, by using a photolysis wavelength of λ = 193 nm, glyoxal possesses very high excess energy. Thus, it is reasonable to assume that the interplay of several electronic states and numerous relaxation processes accounts for the observed pressure effect.

In a previous paper, Zhu et al.[37] determined the absolute quantum yield of HCO following the 193 nm photolysis of glyoxal/nitrogen mixtures at total pressures of 20 Torr < p < 360 Torr. They reported a pressure independent HCO yield of ϕ(HCO) = (0.42 ± 0.21). A possible influence of the HCO forming reaction 4 that might have affected the determined absolute HCO yields and also might have obscured a weak pressure dependence of the HCO quantum yield has not been discussed in their paper. Assuming this pressure independent quantum yield of ϕ(HCO) = 0.42, the ratios *f* measured in our study would correspond to H atom quantum yields of ϕ(H) ≈ 0.67 at p = 20 mbar and ϕ(H) ≈ 1.26 at p = 500 mbar, respectively. Consequently, the main glyoxal photodissociation channels are the HCO radical and H atom forming channels whereas the molecular dissociation pathways with the products H_2, CO, and CH_2O are less important.

3.2. Shock Tube Measurements. HCO was detected in 17 experiments following the photolysis of 0.39% − 1.17% mixtures of glyoxal in argon at temperatures from 769 K < T < 1107 K behind reflected shock waves (0.82 bar < p < 1.84 bar). Whereas the lowest accessible temperature was limited by the operating range of the shock tube, at temperatures higher than 1100 K the thermal decomposition of glyoxal becomes significant.[43] A typical experiment at a temperature of T = 801 K and a pressure of p = 0.9 bar and its sensitivity analysis is shown in Figure 5. The mixture of 1.0% glyoxal was photolyzed with a time delay of 40 μs relative to the arrival time of the reflected shock wave. The photolysis instantaneously yields HCO followed by a short increase of the HCO signal within the first few μs. In contrast to the room-temperature experiments, this increase is not due to the relaxation of excited HCO*, which can be assumed to be complete within less than 1 μs,[45] but a fast formation of HCO radicals by reaction 4. The dotted curve in Figure 5a corresponds to a numerical simulation of the HCO profile that completely neglects reaction 4. Without the steady regeneration of HCO radicals, the resulting HCO lifetime, due to a fast consumption of HCO by H atoms, would be very short.

3.2.1. Reaction H + $(CHO)_2$ at High Temperatures. The experimental high temperature HCO concentration−time profiles were evaluated by assuming an H atom photolysis yield according to the previously determined ratio $f = [H]_0/[HCO]_0^{total}$. Appropriate *f* values were taken from a plot of *f* versus the (normalized) Lennard−Jones collision frequency

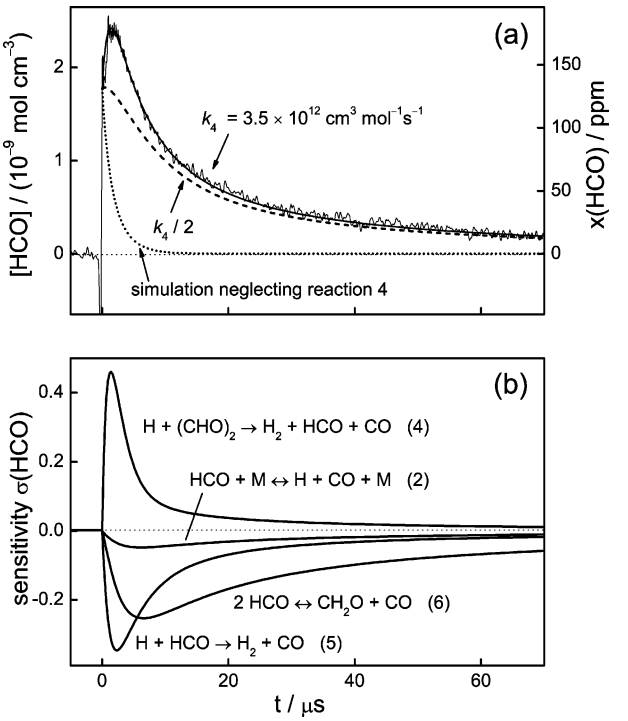

Figure 5. High temperature determination of the rate constant of reaction 4, H + $(CHO)_2$. HCO concentration−time profile (a) and sensitivity analysis (b) for an experiment at $T = 801$ K, $p = 900$ mbar, and 1% glyoxal in Ar. (a) Solid curves: experiment and best fit; dashed curve: simulation with $k_4/2$; dotted curve: simulation neglecting reaction 4.

$Z_{LJ}(T)\rho/Z_{LJ}$ (295 K) as shown in Figure 3.[44] The required Lennard−Jones well depth was estimated from a corresponding value for $Ar(CHO)_2$ to be $\epsilon_{LJ} = 200$ K. At the experimental temperatures and densities used, values of $2.8 < f < 3.1$ were set in the simulations. Due to the fast relaxation of HCO*, the initial $[HCO]_0^{total}$ concentrations could be determined directly from the onset of the HCO profiles. The rate of reaction 4 was used as the adjustable parameter in order to match the experimental HCO profile. All other rate constants were kept fixed at the values given in Table 1. Remaining small positive deviations of the simulated signal at longer reaction times were attributed to a minor contribution of the additional HCO loss reaction

$$HCO + (CHO)_2 \rightarrow \text{products} \qquad (8)$$

Typically, for a best fit of the experiments (solid curve in Figure 5a), the rate constant of reaction 8 was set to $k_8 = k_4/40$. From the sensitivity analysis shown in Figure 5b it is easily seen that the evaluation allowed a sensitive determination of the rate constant of reaction 4. A simulation with the rate constant of reaction 4 decreased by a factor of 2 (dashed curve in Figure 5a) clearly deviates from the experimental profile. The obtained rate constants k_4 are plotted together with the room-temperature result as function of temperature in Figure 6. Different symbols refer to mixtures with different initial glyoxal concentrations. A combined fit of the data, which was constrained to reproduce the room-temperature value, yields the following Arrhenius expression:

$$k_4 = 5.4 \times 10^{13} \times \exp(-18 \text{ kJ mol}^{-1}/RT) \text{ cm}^3 \text{ mol}^{-1} \text{ s}^{-1}$$

$$(\Delta \log k_4 = \pm 0.12)$$

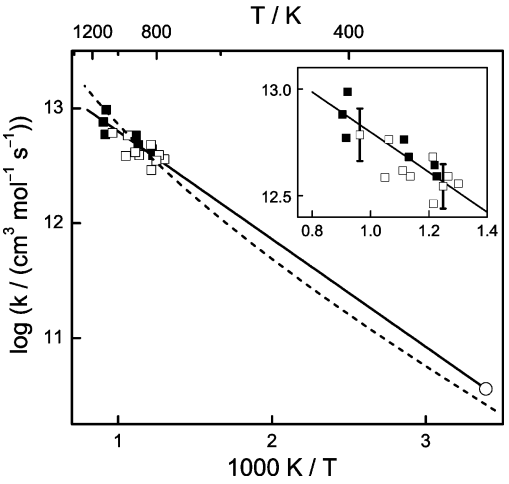

Figure 6. Arrhenius plot of k_4, H + $(CHO)_2$. Different symbols refer to different initial mole fractions of glyoxal in argon: (■) ≈ 0.5% glyoxal, (□) ≈ 1.0% glyoxal, (○) room-temperature measurements with 0.04−1.80% glyoxal. (—) recommended rate expression for k_4, (- -) rate for k_3, H + CH_2O, as given in refs 27 and 28.

The main uncertainty of the determined rate constants stems from the assumed initial H atom yield and initial HCO concentration. The indicated error bars for the high-temperature experiments in Figure 6 correspond to a combined variation of the assumed ratio f, $f \pm 0.5$, and the absolute HCO concentration, $[HCO]_0 \pm 15\%$. The resulting error bars (+32%, − 24%) can be taken as a reasonable absolute error estimate of the measurements. Experimental data and conditions are listed in Table 2S in the Supporting Information.

The dashed curve in Figure 6 refers to a rate expression for reaction 3, H + $CH_2O \rightarrow H_2$ + CO, as it is given by a tunneling corrected TST calculation on a potential energy surface that was characterized with a multireference, configuration interaction calculation.[27] A comparison of the rate expression for reaction 3 and the experimental values for reaction 4 reveals that both the absolute rate constants and the apparent temperature dependence of reactions 3 and 4 are very similar. Both reactions represent simple H atom abstraction reactions from aldehyd groups with comparable bond dissociation enthalpies of the breaking C−H bond, $\Delta H^\circ_{298} = 378$ kJ/mol for reaction 3 versus $\Delta H^\circ_{298} = 357$ kJ/mol for reaction 4. The slight curvature in the Arrhenius plot for reaction 3 is due to tunneling and the importance of two distinct low-frequency saddle point bending modes. A similar temperature dependence can be anticipated for reaction 4; however, in the face of the limited experimental temperature range, a simple Arrhenius fit is adequate for the purpose of this study.

4. The Reaction HCO + O_2

The rate constant of reaction 1, HCO + $O_2 \rightarrow HO_2$ + CO, was determined by a perturbation approach. The well characterized HCO profiles following the photolysis of mixtures of glyoxal in Ar were perturbed by adding controlled levels of O_2 to the reaction mixture. Observed changes in the obtained HCO concentration−time profiles are mainly attributable to the influence of reaction 1. A quasi direct determination of the rate constant of reaction 1 was achieved by adopting the mechanism and rates as elaborated in section 3 without further adjustments and by fitting the observed HCO profiles using only k_1 as adjustable parameter.

4.1. Room-Temperature Measurements. HCO was detected at room temperature following the photolysis of mixtures

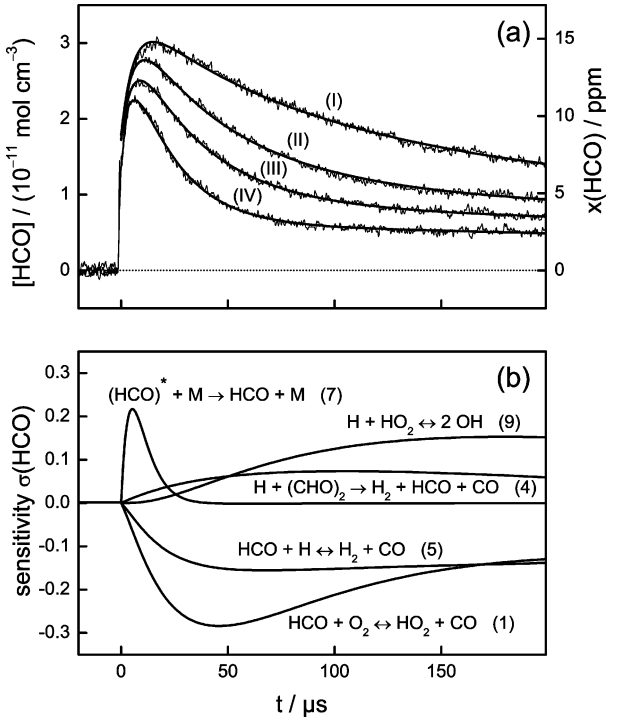

Figure 7. Room temperature determination of the rate constant of reaction 1, HCO + O_2. (a) Sixteen times averaged HCO concentration−time profiles for experiments at $T = 295$ K, $p = 50$ mbar, and 1.14% glyoxal in argon with different initial O_2 mole fractions in the initial mixture: (I) no O_2; (II) 995 ppm O_2; (III) 2005 ppm O_2; (IV) 3985 ppm O_2. (b) Sensitivity analysis for experiment III.

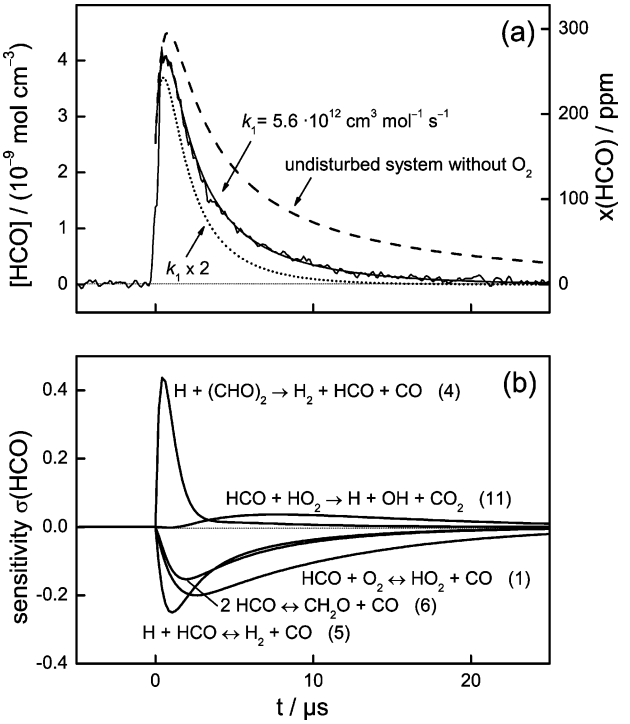

Figure 8. High temperature determination of the rate constant of reaction 1, HCO + O_2. (a) HCO concentration−time profile and (b) sensitivity analysis for an experiment at $T = 857$ K, $p = 1081$ mbar, 2% glyoxal and 3115 ppm O_2 in Ar. (a) Solid curves: experiment and best fit; dotted curve: simulation with $k_1 \times 2$; dashed curve: simulation of the unperturbed system without oxygen.

containing 0.3% to 1.1% glyoxal and 245−3985 ppm O_2 in argon. The total pressure was varied between 50 and 200 mbar. Figure 7a compares four room-temperature experiments with and without addition of different mole fractions of oxygen. As expected, the experiments with added O_2 exhibit a much faster HCO decrease and thus allowed a sensitive determination of the rate constant of reaction 1.

$$k_1(295\ \mathrm{K}) = (3.55 \pm 0.05) \times 10^{12}\ \mathrm{cm^3\,mol^{-1}\,s^{-1}}$$

Here, the error limit corresponds to the error of the mean of 11 measurements based on a 2σ confidence level. Experimental data and conditions are listed in Table 3S in the Supporting Information. Within the scatter of the data, no systematic variations of the determined rate constant at different O_2 mole fractions, initial HCO concentration, initial glyoxal concentration, and total pressure were discernible. Whereas the sensitivity analysis of an experiment with oxygen (Figure 7b) reveals that the observed HCO concentration−time profiles are governed by the rate of reaction 1, at longer reaction times also OH radical chemistry gains in importance. Substantial amounts of HO_2 radicals are generated by reaction 1 such that OH radicals can be subsequently formed through the fast reaction of H atoms with HO_2.

$$\mathrm{H + HO_2 \rightarrow 2\ OH} \qquad (9)$$

Finally, the ensuing abstraction reaction of OH radicals with glyoxal,

$$\mathrm{OH + (CHO)_2 \rightarrow H_2O + HCO + CO} \qquad (10)$$

acts as an additional HCO source. Again, the initially formed (CHO)CO radical can be assumed to thermally decompose within the time-resolution of the experiments. Room-temperature values for the rate constants of the two important reactions 9 and 10 were taken from the IUPAC recommendation,[29] $k_9 = 4.3 \times 10^{13}$ cm^3 mol^{-1} s^{-1}, and from the paper of Plum et al.,[30] $k_{10} = 6.4 \times 10^{13}$ cm^3 mol^{-1} s^{-1}, respectively. It was possible to reproduce the long time behavior of all experimental HCO profiles by a minor, average +12% adjustment of k_9.

4.2. Shock Tube Measurements. High-temperature experiments were performed behind reflected shock waves at temperatures of 739 K < T < 1108 K and pressures of 0.77 bar < p < 1.70 bar using mixtures of 0.53% to 2.0% glyoxal and 1560−3115 ppm oxygen in argon. A time delay of 100 μs was set between the arrival of the shock wave and the photolysis laser pulse. In most experiments, 5% He was added to the reaction mixture in order to shorten the vibrational relaxation time τ_r of oxygen behind the reflected shock wave. With $\tau_r \approx 2.5$ ms at $T = 850$ K and $p = 1$ bar, the vibrational relaxation time of O_2 in Ar is known to be exceedingly long, but it can be efficiently reduced to $\tau_r \approx 60$ μs by addition of 5% He.[46] A further decrease of the relaxation time due to fast vibration−vibration energy transfer between oxygen and glyoxal is expected such that complete vibrational relaxation of O_2 within 100 μs could be assured in any case. Actually, no significant difference of the rate constants determined using mixtures with or without He added could be discerned.

A typical high-temperature experiment is shown in Figure 8. Despite the single-shot character of the shock tube experiments, high quality data were obtained. Overall, the HCO observation times at high temperatures were short. The maximum of the HCO concentration in Figure 8a is reached 0.5 μs after the photolysis laser pulse and the HCO signal reduces to half of its maximum value within 3 μs. In contrast to the room-temperature experiments, no HCO "plateaus" were obtained at longer reaction time. At high temperatures, the additional HCO

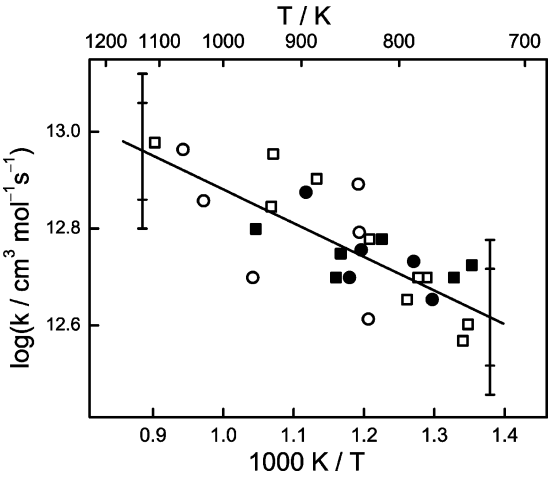

Figure 9. Arrhenius plot of k_1, HCO + O_2. The symbols refer to different initial glyoxal and O_2 mole fractions in Ar: (■) 1−2% glyoxal and 3115 ppm O_2, (□) 1−2% glyoxal and 1560 ppm O_2, (●) ≈ 0.5% glyoxal and 3115 ppm O_2, (○) ≈ 0.5% glyoxal and 1560 ppm O_2. (—) Recommended rate expression for k_1.

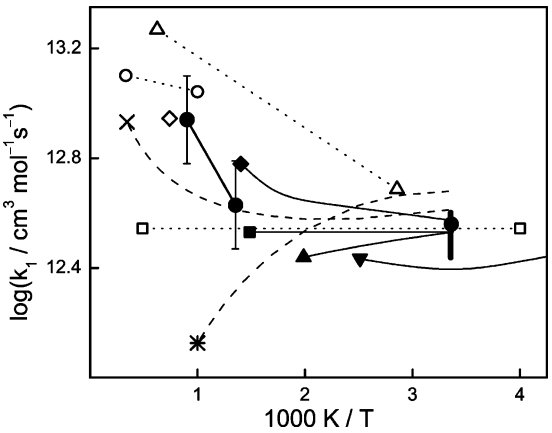

Figure 10. Comparison of the determined room temperature and high-temperature rate constants of reaction 1, HCO + O_2, with selected literature data. Thick vertical bar: room-temperature studies. (△) Vandooren et al.,[47] (○) GRI-Mech 3.0,[16] (◇) de Guertechin et al.,[48] (□) Cherian et al.,[49] (♦) Timonen et al.,[8] (■) DeSain et al.,[9] (▲) Veyret and Lesclaux,[6] (▼) Nesbitt et al.,[7] (×) Hsu et al.,[10] (∗) Bozzelli and Dean,[15] (●) this work. Solid curves: sensitive, direct measurements; dotted curves: indirect measurements; dashed curves: theoretical studies.

regeneration sequence via reactions 9 and 10, due to the weak temperature dependence of both reactions, cannot compete with the dominant HCO loss channels. So far, no experimental data on the temperature dependence of the rate constant of reaction 10 have been reported, however, it can be assumed to be similar to the temperature dependence of the corresponding CH_2O reaction.

A comparison of the sensitivity analyses of the experiments without and with added oxygen, Figures 5b and 8b, reveals that the most important additional reaction with added O_2 is reaction 1 indeed. In particular, reaction 1 dominates the long time behavior of the HCO profile. The importance of the reaction HCO + O_2 is further emphasized by a direct comparison of the experimental HCO profile with a simulation of the undisturbed system by setting the mole fraction of O_2 to zero. Such a simulation is shown as dashed curve in Figure 8a and results in a significantly longer lifetime of HCO than observed experimentally.

Due to the rather high intermediate HCO concentration present in the shock tube experiments, the reaction

$$HCO + HO_2 \rightarrow H + OH + CO_2 \qquad (11)$$

may also gain some importance. Unfortunately, the rate constant and products of reaction 11 are largely unknown. For our analysis, we adopted the assumed products and estimated rate constant $k_{11} = 3.0 \times 10^{13}$ cm^3 mol^{-1} s^{-1} given by Tsang and Hampson.[31] Overall, a data analysis by completely neglecting reaction 11 would have yielded 15% lower rate constants but had a negligible impact on the observed temperature dependence of k_1.

An Arrhenius plot of the determined values for k_1 is shown in Figure 9. Different symbols correspond to measurements performed with different initial glyoxal (≈0.5% and 1.0−2.0%) and oxygen (1560 and 3115 ppm) mole fractions. Within the scatter of the data, no systematic variations of the different data sets are discernible. Overall, a small positive temperature dependence of the rate constant is observed, a linear regression of the data (solid line) reveals an activation energy of E_a = 13.3 ± 4.6 kJ/mol (2σ standard error). In the temperature range 739 K < T < 1108 K the data, which are listed together with the experimental conditions in Table 4S in the Supporting Information, can be represented by the following Arrhenius expression:

$$k_1 = 3.7 \times 10^{13} \exp(-13 \text{ kJ mol}^{-1}/RT) \text{ cm}^3 \text{ mol}^{-1} \text{ s}^{-1}$$

$$(\Delta \log k_1 = \pm 0.16)$$

Again, the main uncertainty of the determined rate constant can be traced back to the uncertainty of the assumed initial ratio $f = [H]_0/[HCO]_0^{total}$ and the absolute HCO concentration. The inner error bars shown in Figure 9 are based on a combined variation of the assumed ratio f, $f \pm 0.5$, and the absolute HCO concentration by ±15%. For a conservative error estimate, allowance has to be made for an additional ±7.5% error due to the assumed rate constant for reaction 11. Finally, a total error of $\Delta \log k_1 = \pm 0.16$ (outer error bars in Figure 9) next to the potential systematic errors also takes into account the statistical scatter of the data.

Throughout this paper, the rate constant of reaction 5, H + HCO, has been assumed to be well-known from our previous studies.[2,328] As can be seen from the sensitivity analyses in Figures 2, 5, 7, and 8, this reaction is one of the most sensitive reactions. Based on a rate constant of $k_5 = 1.1 \times 10^{14}$ cm^3 mol^{-1} s^{-1}, consistent values for the ratio f, k_1, and k_4 were obtained at low and high temperatures. Moreover, in ref 3, the formaldehyde submechanism as outlined in Table 1 was shown to reliably predict almost all formaldehyde pyrolysis literature data, including CH_2O, CO and H atom measurements at temperatures from 1200 to 3200 K with mixtures of 7 ppm to 5% formaldehyde and pressures up to 15 bar. Therefore, to ensure the consistency of the mechanism, changing k_5 from its recommended value is not reasonable without readjusting the rates of other reactions. However, for the purpose of a maximum error estimate, simulations of the experiments using a 25% higher k_5 resulted in 5−12% lower k_1 values.

4.3. Comparison with Literature Data. The determined room temperature and high-temperature rate constants of reaction 1 are compared with selected literature data in Figure 10. The data of this work are represented by filled circles. Reported direct measurements of the rate constant at room temperature (thick vertical bar) span the range from 2.3 × 10^{12}

$cm^3\ mol^{-1}\ s^{-1}$ to $4.0 \times 10^{12}\ cm^3\ mol^{-1}\ s^{-1}$. For a critical assessment of the room-temperature data, we refer to the paper of DeSain et al.[9] These authors argue that most of the reported lower room-temperature rate constants were obtained using a static system and thus were subject to successive photolysis pulses causing a systematic underestimation of the rate constant k_1. Based on their own and eight other direct studies, they support a consensus value of $k_1 \approx 3.4 \times 10^{12}\ cm^3\ mol^{-1}\ s^{-1}$. This value is in excellent agreement with our own determination and confirms the accuracy of the perturbation approach.

The solid curves marked with filled symbols in Figure 10 refer to the results of direct measurements,[6−9] the dotted lines marked with open symbols refer to selected results of flame studies,[47−49] and the dashed curves represent the results of theoretical models.[10,15] The GRI-Mech 3.0 expression is also shown as dotted line marked with open circles.[16] As noted above, direct experimental investigations agree on an overall small temperature dependence of reaction 1 up to a temperature of 700 K, but the reported positive, negligible or negative temperature dependences result in considerable uncertainty of the high-temperature rate constant. The more indirect studies based on the modeling of carbon monoxide[49] and formaldehyde oxidation[1,16,47,48] favor a negligible up to a rather pronounced positive temperature dependence. Theoretical treatments of the association−elimination mechanism with $(CHO)O_2$* as the intermediate also give contrariwise results. A QRRK (quantum Rice−Ramsperger−Kassel) calculation of Bozzelli and Dean[15] predicts a distinctive negative temperature dependence (dashed curve marked with star) whereas the RRKM (Rice−Ramsperger−Kassel−Marcus) calculation of Hsu et al.,[10] which have been performed on an accurate ab initio potential energy surface, results in a nearly temperature independent rate constant (dashed curve marked with cross). Hsu et al. also performed a VTST (variational transition state theory) calculation of the direct H-abstraction channel and found that it significantly contributes to the total rate at high temperatures. According to their study, most of the increase of the reported total rate constant at temperatures $T > 1000$ K can be attributed to the direct abstraction channel.

Our high temperature study extends the range of available sensitive measurements toward high temperatures. The room temperature and shock tube measurements of our work are consistent with a more or less temperature independent rate constant at low temperatures ($T < 700$ K) but also clearly indicate an increase of the observed rate constant at temperatures higher than $T > 700$ K. Whereas the temperature independent rate constant at low temperatures confirms the association−elimination mechanism, the increase of k_1 at high temperatures is probably due to the opening of the direct abstraction channel. Our high-temperature data are compatible with the direct measurements of DeSain et al.[9] and, within the uncertainty limits, also with the results of Timonen et al.[8] Timonen et al. studied reaction 1 in a flow reactor coupled to a photoionization mass spectrometer. Initial HCO concentrations from the photodissociation of CH_3CHO were kept low ($<1 \times 10^{-13}$ mol/cm^3), and the reaction was studied under pseudo first-order conditions. Very similar, DeSain et al.[9] investigated reaction 1 using laser photolysis/cw laser-induced fluorescence. In most of their experiments, initial HCO concentrations of $\sim 3 \times 10^{-11}$ mol/cm^3 were generated photochemically by the reaction of Cl atoms with CH_2O and a temperature independent rate constant of $k_1 = 3.4 \times 10^{12}\ cm^3\ mol^{-1}\ s^{-1}$ was obtained up to temperatures of $T = 673$ K. Experiments using the photodissociation of CH_3CHO and CH_2O as alternative HCO sources were also performed and provided consistent results.

Overall, our data fit well into the picture drawn from the experimental and theoretical studies of Timonen et al., DeSain et al., and Hsu et al. Compared to the theoretical prediction, the somewhat higher experimental k_1 values at high temperatures might indicate an underestimation of the direct abstraction channel by the VTST calculation. Actually, the VTST calculation of the abstraction channel is complicated due to a very small transition state barrier that even disappeared at the level of theory used for the calculations in ref 10.

Interestingly enough, the high-temperature extrapolation of our data also yields a good agreement with most of the flame studies and the GRI-Mech 3.0 expression. For GRI Mech 3.0, the results of shock tube studies on Formaldehyde oxidation reported by Eiteneer et al.[50] and Hidaka et al.[51] served as the main optimization targets to assess the rate of reaction 1. Actually, the rather pronounced positive temperature dependence of k_1 at temperatures $T > 700$ K bridges the gap between the direct low-temperature results and the rather high k_1 values reported in most of the high-temperature flame and shock tube studies.

5. Conclusion

Concentration−time profiles of HCO radicals, which have been generated by a 193 nm excimer laser photolysis of mixtures of glyoxal in argon, were measured using frequency modulation (FM) detection of HCO at a wavelength of $\lambda = 614.752$ nm. The photolysis of glyoxal next to HCO radicals also generates H atoms in high yields. Room temperature experiments showed that the ratio of initially formed H atoms and HCO radicals depend on the total density. H atoms are rapidly transformed into additional HCO radicals by reaction 4, $H + (CHO)_2 \rightarrow H_2 + HCO + CO$. The steady regeneration of HCO radicals turned out to be essential for sufficiently long observation times of HCO behind shock waves. The determined temperature dependence and the absolute rate of reaction 4 are comparable to the rate of the corresponding formaldehyde reaction, $H + CH_2O$. Overall, the 193 nm photolysis of glyoxal due to its high absorption cross section, the high H atom and HCO radical yield, and the HCO regeneration mechanism has been proven to be an efficient source for HCO radicals at high temperatures. The obtained HCO profiles can be well described using an extended reaction mechanism, which is based on a recently validated formaldehyde submechanism.[3]

The rate of the reaction $HCO + O_2 \rightarrow HO_2 + CO$ (1) has been investigated at room temperature and in the temperature range $739\ K < T < 1108$ K behind reflected shock waves employing a perturbation approach. The rate constants were extracted from the observed differences between HCO profiles measured with or without the addition of controlled levels of oxygen. The obtained room-temperature rate constant is in excellent agreement with aivailable literature data. The high-temperature data extend the temperature range of available sensitive rate constant measurements toward higher temperatures and clearly indicate a positive temperature dependence of the rate constant at $T > 700$ K.

Acknowledgment. This work was supported by the Deutsche Forschungsgemeinschaft. We acknowledge Prof. F. Temps for helpful dicussions and advice. G.F. thanks J. V. Michael for providing his shock tube code and R. Signorell, M. Suhm, J. Troe, and H. Gg. Wagner for making available the ring-dye laser system.

Supporting Information Available: Tables of the experimental data and conditions are available free of charge via the Internet at http://pubs.acs.org.

References and Notes

(1) Glarborg, P.; Alzueta, M. U.; Kjærgaard, K.; Dam-Johansen, K. *Combust. Flame* **2003**, *132*, 629.

(2) Friedrichs, G.; Herbon, J. T.; Davidson, D. F.; Hanson, R. K. *Phys. Chem. Chem. Phys.* **2002**, *4*, 5778.

(3) Friedrichs, G.; Davidson, D. F.; Hanson, R. K. *Int. J. Chem. Kinet.* **2004**, *36*, 157.

(4) Hippler, H.; Krasteva, N.; Striebel, F. *Phys. Chem. Chem. Phys.* **2004**, *6*, 3383, and **2005**, *9*, 2074 and **2005**, *9*, 2077.

(5) Krasnoperov, L. N.; Chesnokov, E. N.; Stark, H.; Ravishankara, A. R. *J. Phys. Chem. A* **2004**, *108*, 11526.

(6) Veyret, B.; Lesclaux, R. *J. Phys. Chem.* **1981**, *85*, 1918.

(7) Nesbitt, F. L.; Gleason, J. F.; Stief, L. J. *J. Phys. Chem. A* **1999**, *103*, 3038.

(8) Timonen, R. S.; Ratajczak, E.; Gutman, D. *J. Phys. Chem.* **1988**, *92*, 651.

(9) DeSain, J. D.; Jusinski, L. E.; Ho, A. D.; Taatjes, C. A. *Chem. Phys. Lett.* **2001**, *347*, 79.

(10) Hsu, C.-C.; Mebel, M.; Lin, M. C. *J. Chem. Phys.* **1996**, *105*, 2346.

(11) Temps, F.; Wagner, H. Gg. *Ber. Bunsen-Ges. Phys. Chem.* **1984**, *88*, 410.

(12) Yamasaki, K.; Sato, M.; Itakura, A.; Watanabe, A.; Kakuda, T.; Tokue, I. *J. Phys. Chem. A* **2000**, *104*, 6517.

(13) Langford, A. O.; Moore, B. *J. Phys. Chem.* **1977**, *81*, 2292.

(14) Langford, A. O.; Moore, B. *J. Chem. Phys.* **1984**, *80*, 4211.

(15) Bozzelli, J. W.; Dean, A. M. *J. Phys. Chem.* **1993**, *97*, 4427.

(16) Smith, G. P.; Golden, D. M.; Frenklach, M.; Moriarty, N. W.; Eiteneer, B.; Goldenberg, M.; Bowman, C. T.; Hanson, R.; Song, S.; Gardiner, W. C., Jr.; Lissianski, V.; Qin, Z. *GRI-Mech Version 3.0*, 1999, http://www.me.berkeley.edu/gri_mech.

(17) Orlando, J. J.; Tyndall, G. S. *Int. J. Chem. Kinet.* **2001**, *33*, 149.

(18) Klatt, M. *Quantitative Untersuchung der Bildung und des Verbrauchs von H− und O−Atomen sowie OH−Radikalen in verschiedenen Elementarreaktionen bei hohen Temperaturen*, Ph.D. Thesis, Universität Göttingen, 1991.

(19) Konnov, A. A. *Detailed reaction mechanism for small hydrocarbons combustion. Release 0.5*, 2000, http://homepages.vub.ac.be/∼akonnov.

(20) Frenkel, M. *Thermodynamics of Organic Compounds in the Gas State*; Thermodynamics Research Center: College Station, TX, 1994.

(21) Colberg, M.; Friedrichs, G. *Characterization of a Low-Pressure Shock Tube by Kinetic Measurements of the Thermal Decomposition of Ammonia and Methylamine*, in preparation.

(22) Michael, J. V.; Sutherland, J. W. *Int. J. Chem. Kinet.* **1986**, *18*, 409.

(23) Michael, J. V. *J. Chem. Phys.* **1989**, *90*, 189.

(24) Davidson, D. F.; Chang, A. Y.; Hanson, R. K. *Proc. Combust. Inst.* **1988**, *22*, 1877.

(25) Deppe, J.; Friedrichs, G.; Römming, H.-J.; Ibrahim, A.; Wagner, H. Gg. *Ber. Bunsen-Ges. Phys. Chem.* **1998**, *102*, 1474.

(26) Friedrichs, G.; Wagner, H. Gg. *Z. Phys. Chem.* **2000**, *214*, 1723.

(27) Irdam, E. A.; Kiefer, J. H.; Harding, L. B.; Wagner, A. F. *Int. J. Chem. Kinet.* **1993**, *25*, 285.

(28) Friedrichs, G.; Davidson, D. F.; Hanson, R. K. *Int. J. Chem. Kinet.* **2002**, *34*, 374.

(29) Atkinson, R.; Baulch, D. L.; Cox, R. A.; Hampson, R. F. J.; Kerr, J. A.; Rossi, M. J.; Troe, J. *J. Phys. Chem. Ref. Data* **1997**, *26*, 1329.

(30) Plum, C. N.; Sanhueza, E.; Atkinson, R.; Carter, W. P. L.; Pitts, J. N., Jr. *Environ. Sci. Technol.* **1983**, *17*, 479.

(31) Tsang, W.; Hampson, R. F. *J. Phys. Chem. Ref. Data* **1986**, *15*, 1087.

(32) Baulch, D. L.; Cobos, C. J.; Cox, R. A.; Esser, C.; Frank, P.; Just, T.; Kerr, J. A.; Pilling, M. J.; Troe, J.; Walker, R. W.; Warnatz, J. *J. Phys. Chem. Ref. Data* **1992**, *21*, 411.

(33) Timonen, R. S.; Ratajczak, E.; Gutman, D.; Wagner, A. *J. Phys. Chem.* **1987**, *91*, 5325.

(34) Hippler, H.; Krasteva, N.; Striebel, F. *6th International Conference on Chemical Kinetics*; NIST: Gaithersburg, MD, 2005, Abstract J1.

(35) Kee, R. J.; Ruply, F. M.; Miller, J. A. *Chemkin-II: A Fortran Chemical Kinetics Package for the Analysis of Gas-Phase Chemical Kinetics*; Sandia Report SAND89-8009, Sandia National Laboratories: Livermore: CA, 1989, http://www.ca.sandia.gov/chemkin/.

(36) Chen, Y.; Zhu, L. *J. Phys. Chem. A* **2003**, *107*, 4643.

(37) Zhu, L.; Kellis, D.; Ding, C.-F. *Chem. Phys. Lett.* **1996**, *257*, 487.

(38) Moortgat, G. K.; Warneck, P. *J. Chem. Phys.* **1979**, *70*, 3639.

(39) Meller, R. E.; Moortgat, G. K. *J. Geophys. Res.* **2000**, *105*, 7089.

(40) Langford, A. O.; Moore, B. *J. Chem. Phys.* **1984**, *80*, 4202.

(41) Curtiss, L. A.; Raghavachari, K.; Redfern, P. C.; Rassolov, V.; Pople, J. A. *J. Chem. Phys.* **1998**, *109*, 7764.

(42) Förgeteg, S.; Bérces, T.; Dóbé, S. *Int. J. Chem. Kinet.* **1979**, *11*, 219.

(43) Saito, K.; Kakumoto, T.; Murakami, I. *J. Phys. Chem.* **1984**, *88*, 1182.

(44) Hischfelder, J. O.; Curtiss, C. F.; Bird, R. B. *Molecular Theory of Gases and Liquids*; Wiley: London, 1954.

(45) Millikan, R. C.; White, D. R. *J. Chem. Phys.* **1963**, *39*, 3209.

(46) Rao, V. S.; Skinner, G. B. *J. Chem. Phys.* **1984**, *81*, 775.

(47) Vandooren, J.; de Guertechin, L. O.; Van Tiggelen, P. J. *Combust. Flame* **1986**, *64*, 127.

(48) de Guertechin, L. O.; Vandooren, J.; Van Tiggelen, P. J. *Bull. Soc. Chim. Belg.* **1983**, *92*, 663.

(49) Cherian, M. A.; Rhodes, P.; Simpson, R. J.; Dixon-Lewis, G. *Proc. Combust. Inst.* **1981**, *18*, 385.

(50) Eiteneer, B.; Yu, C.-L.; Goldenberg, M.; Frenklach, M. *J. Phys. Chem.* **1998**, *102*, 5196.

(51) Hidaka, Y.; Taniguchi, T.; Tanaka, H.; Kamesawa, T.; Inami, K.; Kawano, H. *Combust. Flame* **1993**, *92*, 365.